

# Picosecond Multidimensional Fluorescence Spectroscopy: A Tool to Measure Real-time Protein Dynamics During Function<sup>†</sup>

Tai-Yang Kim, Kathrin Winkler and Ulrike Alexiev\*

Department of Physics, Freie Universität Berlin, Arnimallee 14, D-14195 Berlin, Germany

Received 21 June 2006; accepted 20 November 2006; published online 21 November 2006; DOI: 10.1562/2006-06-21-RA-943

## ABSTRACT

Advanced multidimensional time-correlated single photon counting (mdTCSPC) and picosecond time-resolved fluorescence in combination with site-directed fluorescence labeling are valuable tools to study the properties of membrane protein surface segments on the pico- to nanoseconds time scale. Time-resolved fluorescence anisotropy changes of protein bound fluorescent probes reveal changes in protein dynamics and steric restriction. In addition, the change in fluorescence lifetime and intensity of the covalently bound fluorescent dye is indicative of environmental changes at the protein surface. In this study, we have measured the changes in fluorescence lifetime traces of the fluorescent dye fluorescein covalently bound to the first cytoplasmic loop of bacteriorhodopsin (bR) after light activation of protein function. The fluorescence is excited by a picosecond laser pulse. The retinylidene chromophore of bR is light-activated by a 10 ns laser pulse, which in turn triggers recording of a sequence of fluorescence lifetime traces in the mdTCSPC-module. The fluorescence decay changes upon protein function occur predominantly in the 100 ps time range. The kinetics of these changes shows two transitions between three intermediate states in the second part of the bR photocycle. Correlation with photocycle kinetics allows for the determination of reaction intermediates at the proteins surface which are coupled to changes in the retinal binding pocket.

## INTRODUCTION

Dynamics and conformational changes of proteins occur on a range of time scales, from subpicoseconds to seconds or even longer. Ultrafast UV/VIS, infrared and two-dimensional infrared spectroscopy provide information from femtoseconds (*e.g.* thermal fluctuation within conformational states and photo-isomerization of ligands) up to picoseconds (*e.g.* fast peptide backbone conformational changes) (1,2). The understanding of protein dynamics is of general importance for the elucidation of mechanisms involved not only in protein function but also in protein folding. An important issue in protein folding and for conformational changes during protein function is the rate at which a polypeptide chain can explore conformational space. The conformational

search within a polypeptide chain is limited by intrachain diffusion processes on the subnanosecond to microsecond time scale (3).

Conformational changes within and at the surface of the 7 transmembrane helical proteins bacteriorhodopsin, visual rhodopsin and sensory rhodopsin were elucidated using various techniques comprising X-ray studies and electron crystallography on trapped intermediates, as well as time-resolved EPR, different NMR-techniques, fluorescence spectroscopy and mutagenesis studies (4–21). However, the exact nature of the molecular mechanisms underlying these conformational changes, their magnitude and their occurrence during the time course of the photoreactions are still largely unclear. Time-resolved fluorescence depolarization techniques are appropriate to investigate under physiological conditions the diffusional dynamics and conformational changes of peptides and protein segments on the picosecond to nanosecond time scale. On this time scale, the dynamics of surface loops of membrane proteins are expected to occur (20,21). In addition, quenching methods like photo-induced electron transfer between a fluorescent dye and an intrinsic tryptophan provide information about small-scale conformational changes, as any change in conformation or flexibility effects change in fluorescence intensity and lifetime (22–24). Therefore, we implemented a new two-dimensional time-resolved fluorescence apparatus to measure the time-resolved fluorescence of protein surface attached fluorescence probes during the time course of protein function. This experimental setup combined with site-specific labeling allows us to map the entire protein surface providing time-dependent protein dynamics maps with a detailed picture of surface conformational or environmental changes. Analysis of the surface dynamics maps allows for the determination of all intermediates of reactions, which take place on the receptor surface upon activation or interaction with the signal proteins. In this respect, this multidimensional fluorescence method described here is complementary to time-resolved X-ray crystallography (25).

We first set out to measure the change in fluorescence lifetime of a fluorescent probe covalently attached to the cytoplasmic surface of bacteriorhodopsin. This experiment was inspired by the observation that an increase in fluorescence intensity of a fluorescent dye covalently bound to the cytoplasmic surface of visual rhodopsin occurs upon light-activation of rhodopsin and scales with the amount of the active receptor formed (6).

<sup>†</sup>This paper is part of the Proceedings of the 12th International Conference on Retinal Proteins held at Awaji Island, Hyogo, Japan on 4–8 June 2006.

\*Corresponding author email: alexiev@physik.fu-berlin.de (Ulrike Alexiev)  
© 2007 American Society for Photobiology 0031-8655/07

## MATERIALS AND METHODS

**Sample preparation.** The preparation and expression of the bR mutant protein S35C in *Halobacterium salinarum*, in which cysteine replaces serine 35, has been reported (20,26). Labeling of bR with 5-(iodoacetamido)-fluorescein (IAF, Molecular Probes) and the determination of the labeling stoichiometry were performed as described (20). In brief, the reaction of 50  $\mu\text{M}$  bR with 2 mM fluorescent label was carried out at room temperature in 150 mM KCl, 100 mM Tris-HCl (pH 8.0), 30 mM ethylenediaminetetraacetic acid (EDTA), 200  $\mu\text{M}$  dithiothreitol (DTT) for 10 min. A 10 mM stock solution of the label was used. The labeling stoichiometry was calculated using:

$$\frac{c_{\text{Label}}}{c_{\text{bR}}} = \left( \frac{\Delta A_{\text{L}}}{\epsilon_{\text{L}}} \right) \left( \frac{\epsilon_{\text{bR}}}{A_{568}} \right) \quad (1)$$

$c_{\text{Label}}$  and  $c_{\text{bR}}$  are the molar concentrations of the bound fluorescent label and bR, respectively.  $\Delta A_{\text{L}}$  is the absorbance difference at the peak of the absorption band ( $\lambda_{\text{max}}$ ) of the label.  $\epsilon_{\text{L}}$  is the molar extinction coefficient of the label (from Molecular Probes).  $A_{568}$  is the absorbance of the bR sample at 568 nm with the molar extinction coefficient  $\epsilon_{\text{bR}} \approx 63,000 \text{ M}^{-1} \text{ cm}^{-1}$ .

**Flash spectroscopy.** Flash spectroscopy and data analysis with a sum of exponentials were performed as described (27,28). The excitation was with 10 ns pulses of  $\sim 10 \text{ mJ cm}^{-2}$  at 493 nm. Under these conditions about 20–30% of bR molecules are cycling. Typically, 30–50 traces were averaged for the kinetics of the bR photocycle detected at different wavelengths between 390 and 670 nm.

**Stationary fluorescence spectroscopy.** Steady-state fluorescence experiments were carried out using a Jobin-Yvon Spex Fluoromax single photon counting spectrofluorimeter.

**Time-resolved fluorescence spectroscopy and data analysis.** The bR-photocycle induced fluorescence changes of fluorescein covalently bound to the cysteine in position 35 (S35C-AF) on the cytoplasmic surface were determined in purple membrane suspensions containing 10  $\mu\text{M}$  bR-S35C-AF in 150 mM KCl, 10 mM Tris pH 7. In order to measure fluorescence changes due to environmental changes and not due to light-induced proton concentration changes caused by proton uptake, the fluorescence lifetime traces were recorded in buffered solution. The buffer (10 mM Tris) used had no effect on the photocycle kinetics (27).

A description of the classic Titan-Sapphire laser based TCSPC setup was already given (20). The fluorescence decay profiles  $I(t)$  were analyzed using the software package Global Unlimited V2.2 (Laboratory for Fluorescence Dynamics, University of Illinois). The time-course of the fluorescence was fitted with a sum of exponentials:

$$I(t) = \sum_{i=1} \alpha_i \cdot e^{-t/\tau_i} \quad (2)$$

## RESULTS

### Characterization of fluorescently labeled bR

**Spectral properties.** Under the conditions described in Materials and Methods, 0.1 mol of IAF was selectively bound per mol bR to the cysteine in position 35 of the AB-loop at the cytoplasmic surface. At this labeling stoichiometry, almost no homo energy transfer occurs between the fluorescent dyes attached to neighboring bacteriorhodopsin molecules in the purple membrane. The absorbance and emission spectra of the fluorescein labeled bR mutant protein, S35C-AF, are shown in Fig. 1. Fluorescein has a pH-sensitive absorption band with a maximum at  $\lambda_{\text{max}} = 492 \pm 1 \text{ nm}$  in the alkaline form for IAF-labeled bR molecules in isolated purple membranes. Due to the low labeling stoichiometry and pH 7 of the buffer solution the fluorescein absorption band appears as a shoulder (marked with arrow (2)) in the absorbance spectrum of bR-S35C-AF (arrow (1)). The emission spectrum of bound fluorescein with  $\lambda_{\text{max}} = 513 \pm 1 \text{ nm}$  (arrow (3)) is shown in the inset of Fig. 1.

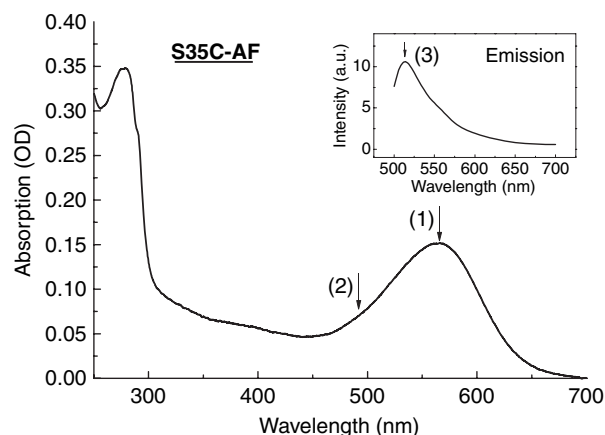


**Figure 1.** Absorption and emission spectra of the IAF labeled bacteriorhodopsin mutant S35C (S35C-AF). The fluorophore is bound to the single cysteine residue at position 35 in the AB-loop of bacteriorhodopsin. Conditions: 150 mM KCl, 10 mM Tris pH 7 at 10°C.

**Photocycle kinetics.** Bacteriorhodopsin acts as a light-driven proton pump in the plasma membrane of *H. salinarum*. A retinylidene chromophore is bound *via* a protonated Schiff base linkage to Lys216. In the first half of the photocycle, the Schiff base becomes deprotonated during the transition to the M-intermediate and in the same time range a proton is released at the extracellular surface. During the second half of the photocycle, the Schiff base is reprotonated from Asp96, which is located in the cytoplasmic part of the protein, and a proton is taken up from the cytoplasm. Formation and decay of the M-intermediate thus correspond to deprotonation and reprotonation of the Schiff base during the photocycle. The photocycle was measured at 17 wavelengths between 390 and 670 nm. Fig. 2 shows the photocycle kinetics of S35C-AF measured in 150 mM KCl at pH 7 and 10°C at three different wavelengths (410, 570 and 650 nm), which are diagnostic for the kinetics of the M- intermediate (410 nm), K- and O-intermediates (650 nm), and the depletion signal (570 nm).

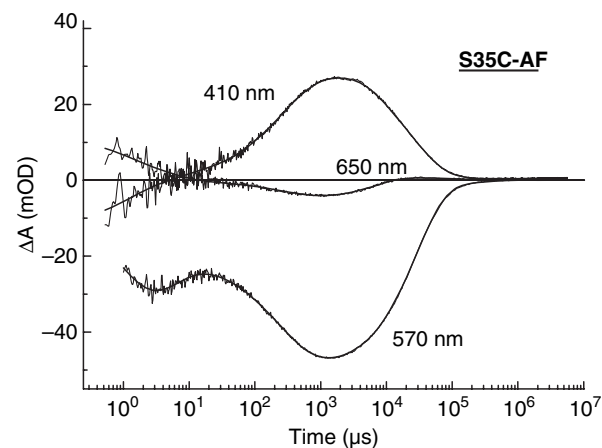


**Figure 2.** Time course of the light-induced differential absorbance of S35C-AF at 410, 570 and 650 nm. The time courses were globally fitted with a sum of eight exponentials and the fits are shown as lines. Conditions as in Fig. 1.

A multiexponential global fit of the photocycle with eight exponentials results in the following apparent time constants 1.1/5.4/79/306  $\mu\text{s}$  and 1.7/6.3/29/212 ms.

### Fluorescence pump-probe measurements

*Experimental setup.* We implemented a tunable laser/micro-channel plate based home-built apparatus for mdTCSPC with picosecond time-resolution to measure time-resolved fluorescence intensity decays during protein function with microsecond time-resolution. In the following, a brief description of this experiment is given and the schematic setup is illustrated in Fig. 3.

The sample fluorescence was excited with the second harmonic (LBO crystal, Frequency Doubler, Spectra Physics) of a Ti:sapphire laser (Millenia Vs and Tsunami, Spectra Physics) at a repetition rate of 4.05 MHz [*Probe Laser*]. The output power was 200  $\mu\text{W}$ –1 mW at wavelengths in the range between 355 and 500 nm. The pulse width was 1.5–2 ps full width at half maximum (FWHM). The laser output remained stable over several hours. The linearly horizontally polarized second harmonic was passed through an achromatic Fresnel rhomb [*FR*] to rotate the plane of polarization.

- (1) A fraction of the light was directed onto a nanosecond-photodiode (DET210, Thorlabs). The resulting positive electronic pulse was amplified with a 1.6 GHz preamplifier (HFAC-26, B&H GmbH) [*Preamp*] and converted to negative. The negative amplified photodiode pulse (set to  $-0.5$  V by a variable neutral density filter [*F*] in front of the diode to correct for the different laser output intensities at the various wavelength) was passed directly into the TCSPC Module (SPC-830, B&H GmbH), which is a pci-card installed into a PC. The Constant Fraction Discriminators (CFDs), the Time-to-Amplitude Converter (TAC), a fast Analog-to-Digital Converter (ADC) and the Multichannel Analyser (MCA) with the data memory and the associated control circuits are integrated on the board.

(2) The excitation light pulse was passed through two neutral density filters, mounted into a double multiple filter wheel [*DF*], which enables one to set two of 12 filters in position. In this way, the intensity of the excitation light could be coarsely and finely attenuated in order to achieve proper counting statistics. Before hitting the sample, the light was passed through a Glan-Thompson polarizer [*GP*] (set to produce a vertically polarized output) and a dispersing lens [*DL*]. The typical excitation powers were in the nW range, low enough to ensure single photon counting (in the range of  $\text{fJ cm}^{-2}$ ). The fluorescence was collected at right-angles. The cuvette-holder for the sample is temperature controlled and contains a fiberoptic connector for the pump laser beam.

(3) The fluorescence emission was detected after passing through a cut-off color glass filter [*CO*] (OG 515 for the sample containing fluorescein) or a suitable neutral density filter (for the reference), a lens [*L*], an iris diaphragm [*I*], a sheet polarizer [*P*] and an electronically controlled shutter [*Sh*] (LS6T2K, Uniblitz) onto a micro-channel plate photomultiplier tube [*MCP*] (R3809U, Hamamatsu). The sheet polarizer was set to  $54.7^\circ$  (“magic angle”) for the fluorescence lifetime measurements.

(4) The fluorescence emission was detected after passing through a cut-off color glass filter [*CO*] (OG 515 for the sample containing fluorescein) or a suitable neutral density filter (for the reference), a lens [*L*], an iris diaphragm [*I*], a sheet polarizer [*P*] and an electronically controlled shutter [*Sh*] (LS6T2K, Uniblitz) onto a micro-channel plate photomultiplier tube [*MCP*] (R3809U, Hamamatsu). The sheet polarizer was set to  $54.7^\circ$  (“magic angle”) for the fluorescence lifetime measurements.

The MCP operated at  $-2.84$  kV. The dark counts were reduced to less than 10 Hz using a thermoelectric cooled housing. The MCP output was amplified with a 1.6 GHz preamplifier (HFAC-26, B&H GmbH) and passed into the TCSPC Module. The ratio of the stop/start pulse rate was normally less than 200:1, appropriate for single photon counting.

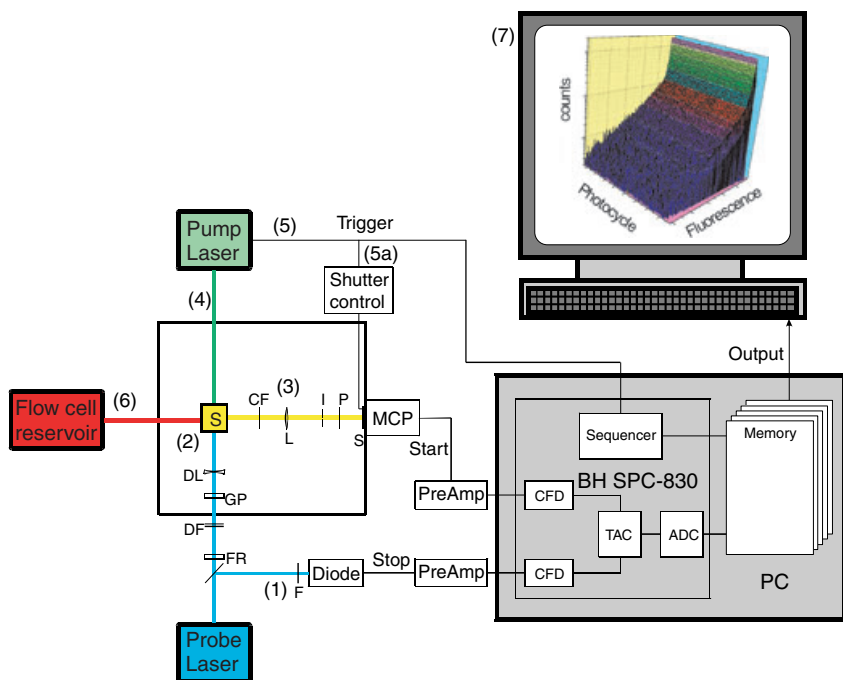


**Figure 3.** Scheme of the multidimensional TCSPC setup. For a detailed description see the Results section.

The channel width of the MCA could be varied, but data were collected in 1024 channels. The fluorescence decay data were stored with the software provided with the SPC module, converted and used for data analysis.

The instrumental response function (IRF) was determined at the corresponding wavelengths with LUDOX (Grace), a colloidal silica solution, as a scattering material. The IRF of the system was typically about 40 ps (FWHM) at a channel width of 20 ps as well as 30 ps at a channel width of 3 ps.

- (4) Flash photolysis of bacteriorhodopsin was achieved by using a 10 ns light pulse of an excimer laser (EMG 50, Lambda Physik – 90 mJ output energy at 308 nm) pumped dye laser (with Coumarin 307 in EtOH – 16 mJ output energy at 493 nm) [*Pump Laser*]. The laser light was guided through a glass fiber (Ocean Optics) into the cuvette-holder. The output energy/area at the end of the fiber was 3–5 mJ cm<sup>-2</sup>.
- (5) The power supply of the excimer laser has an electronic trigger output which triggers the sequencer on the TCSPC-board and also the home-built shutter control. The shutter control opens the shutter for a defined time-interval (5a).
- (6) The sample [*S*] bacteriorhodopsin was measured in a 3 × 3 mm quartz cuvette. The repetition rate of the excimer laser to excite the photocycle was set to 0.4 Hz. To excite samples with noncyclic protein-function, like visual rhodopsin not undergoing a photocycle, a flow cell can be used [*Flow cell*]. In this case, the sample reservoir resides in a dark box to avoid light exposure of the sample.
- (7) Sequence of fluorescence lifetime traces during the bacteriorhodopsin photocycle.

**Fluorescence lifetime changes during bR photocycle.** We have measured the changes in excited state fluorescence decay of S35C-AF with 2 ms time-resolution during the bR-S35C-AF photocycle. In the dark state of S35C-AF, three decay components were necessary to fit the fluorescence lifetime curve of the covalently attached fluorescein (0.16/1.2/4.0 ns) (Fig. 4), while

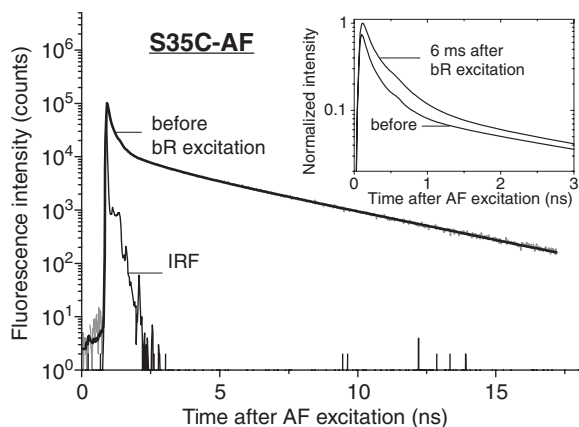


**Figure 4.** Time-course of fluorescence intensity decay of bR-S35C-AF. The instrumental response function (IRF) of the experimental setup is shown. The time course was fitted according to Eq. (2) and the fit is shown as a line. Inset: comparison of the fluorescence decays before and 6 ms after light-excitation of the S35C-AF photocycle. Conditions as in Fig. 1. The excitation was as 470 nm, the fluorescence emission was detected after passing through a cut-off color glass filter OG515.

fluorescein free in solution exhibits only one fluorescence lifetime component of  $\sim 4$  ns. These values agree with earlier observations on S35C-AF incorporated in mixed micelles (20). To observe the changes in time-resolved fluorescence during the bacteriorhodopsin photocycle, we monitored a series of 500 sequential time-resolved fluorescence decays after flash activation of the S35C-AF photocycle (see also Fig. 3 [7]). The fluorescence decay curves in the dark state of S35C-AF and 6 ms after flash activation of the photocycle are compared in the inset of Fig. 4. Fig. 5b shows the difference contour plot between the fluorescence lifetime traces measured during the S35C-AF photocycle and the lifetime trace measured before S35C-AF photocycle excitation. The highest increase in fluorescence intensity (marked with a “+”) during the bR-S35C-AF photocycle occurs predominantly with the fastest fluorescence lifetime component in the 0.1–0.2 ns range. For comparison, a contour plot of the S35C-AF photocycle (Fig. 5a) is presented. In this figure the absorbance increase due to the M-intermediate is marked with a “+”. Virtually, the increase in fluorescence intensity is present during the lifetime of the M-intermediate. Two main transitions were observed for the M-decay with time constants of 5 and 30 ms (fit of the photocycle time trace measured at 410 nm), which roughly matches those of the fluorescence decrease with 11 and 44 ms (Fig. 5c). The 5 ms M-decay component from the fit of the absorption change at a single wavelength compares to the 6.3 ms time constant from the global fit of the photocycle (see Fig. 2). This time constant describes mainly the M  $\rightarrow$  N/O transition (see also Fig. 2). As the formation of the O-intermediate is favored at higher temperatures and acidic pH-values (29), the amplitude of the 5-ms decay component at 10°C and pH 7 amounts only to 16% of the total amplitude, consistent with a 10–30% accumulation of the O-intermediate at 10°C. A closer look at the amplitudes of the fluorescence intensity change kinetics at 166 ps after fluorescence excitation (Fig. 5c), however, reveals that the fluorescence decrease is slightly faster than the decay of the M-intermediate.

## DISCUSSION

In this report, we describe the experimental setup for the detection of fast fluorescence lifetime changes and the application to fluorescently labeled bacteriorhodopsin. Because of the presence of different quenching and energy transfer rates, the fluorescence decays observed at the surface of fluorescently labeled rhodopsins are multiexponential and range from about 30 ps to several nanoseconds (20,30). As the fluorescence lifetime of an excited fluorescent dye is mostly independent of its concentration, but depends on the interaction with the local environment, fluorescence lifetime transients contain information about the different states of interaction of fluorescent species with their environment (31). A suitable technique to monitor *changes* in fluorescence lifetime during protein function with microsecond time resolution is the recently introduced multidimensional TCSPC technique (32), which was used to record fast dynamic changes in the fluorescence behavior of a sample (33). Here, the successful implementation of an experimental setup consisting of a multidimensional TCSPC module, a high-repetition rate tunable picosecond laser system and a coupling device for a further laser system, which provides nanosecond excitation pulses is demonstrated.

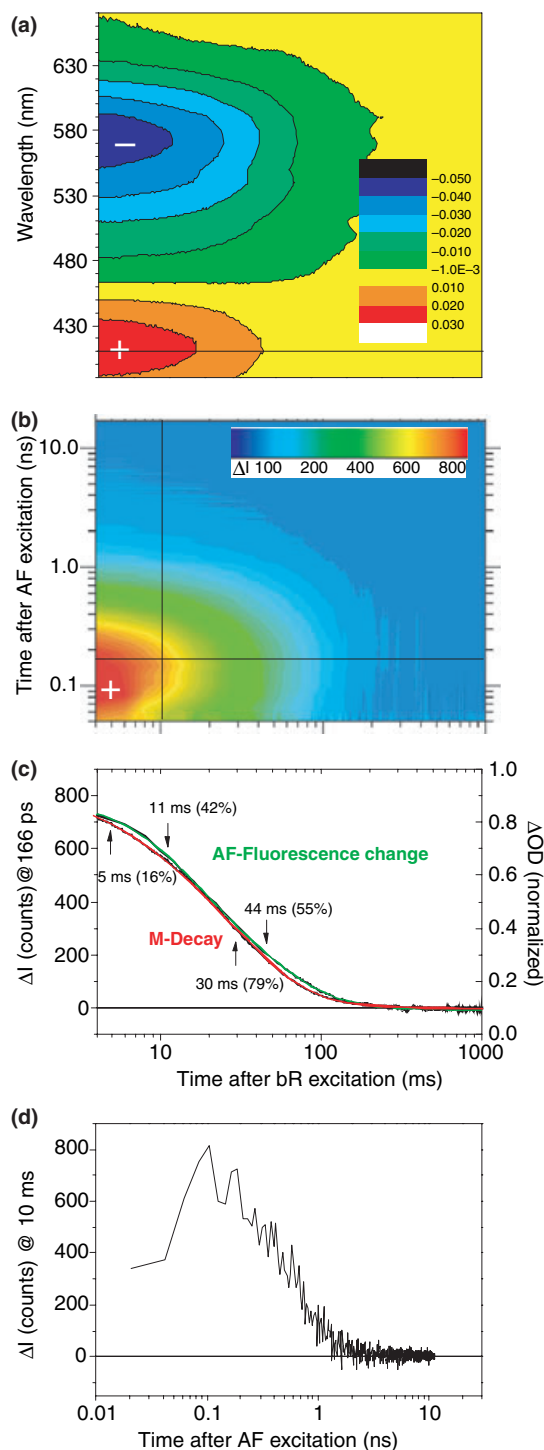


**Figure 5.** Comparison of S35C-AF photocycle kinetics and kinetics of fluorescence lifetime changes. Panel a: contour plot of the absorbance changes between 390 and 670 nm during the S35C-AF photocycle. Panel b: contour plot of the AF fluorescence intensity changes during the S35C-AF photocycle as a function of time after fluorescence excitation. The color coding bar represents the changes in fluorescence intensity  $\Delta I$ . Panel c: comparison of normalized, light-induced AF fluorescence changes at 166 ps after AF excitation and absorbance changes at 410 nm (M-intermediate). The time traces are indicated by horizontal lines in the contour plots in panels a and b. Panel d: AF fluorescence change at 10 ms after light-activation of S35C-AF. The time trace is indicated by vertical lines in the contour plot in panel b. Conditions as in Fig. 4.

Flash photolysis of the fluorescently labeled bR mutant protein S35C-AF (10% AF incorporation) with nanosecond pulses revealed a similar kinetic behavior of the S35C-AF photocycle to that found for wild type under similar conditions (data not shown). This finding agrees with earlier results on S35C-AF (70–100% AF incorporation), where the M-intermediate time trace coincides with wild type (34).

The fluorescence decay changes observed during the second half of the bR photocycle at the cytoplasmic surface are indicative for interactions of the fluorescent dye with its environment. During the second half of the photocycle, comprising the N- and O-intermediates, the Schiff base is reprotonated from Asp96, which is located in the cytoplasmic part of the protein, and a proton is taken up from the cytoplasm. From various studies it is evident that in the late M and N states the cytoplasmic end of helix F moves outward, the conformation of the EF loop changes and helix G tilts towards the proton channel (11,13,14). The fluorescent probe at position S35C in the AB-loop is located next to helix G and thus in a good position to sense environmental changes connected with helix G.

In addition to the environment-induced fluorescence changes, fluorescence resonance energy transfer (FRET) from the excited fluorescent dye fluorescein to the retinal can be expected from the spectral overlap of AF fluorescence and bR chromophore absorption (Fig. 1). In control measurements without energy transfer we used a bR sample with a reduced Schiff base linkage (rR–bR), which results in a blue shift of the retinal absorption ( $\lambda_{\max} \sim 350$  nm). The experiments with rR–bR revealed that mainly the fast ( $\sim 0.1$  ns) and the slow ( $\sim 4$  ns) fluorescence decay components are involved in energy transfer ((20), Alexiev *et al.*, unpublished data). The relative amplitude of the 0.1 ns component decreases from about 70% in bR to 20% in rR–bR without FRET. In the M intermediate no energy transfer from the excited fluorescein to the retinal occurs because of the shift in the chromophore absorbance maximum to 412 nm. If the observed fluorescence changes during the photocycle were due to the change in FRET, we would expect a decrease in the amplitude of the fast ( $\sim 0.1$  ns) fluorescence decay component in the M-intermediate. In the experiments reported here, however, an increase of this amplitude was observed in the M-intermediate, in contrast to the expectations for FRET based fluorescence changes. In addition, a general increase of the amplitudes of all three fluorescence lifetime components occurs during the M-intermediate. The 0.1 ns fluorescence decay component experiences the largest increase in total amplitude (see Fig. 5d). This indicates that the fluorescence changes detected at position 35 originate rather from environmental changes at the surface than from energy transfer to the retinal or from both.

The decay of the fluorescence increase is slightly slower than the decay of the M-intermediate. The small differences seen remain to be explained in future work. Interestingly, a similar result was found in experiments with spin-labels attached to position 35 (35). The EPR spectral change for the labeled S35C mutant decays with a slightly slower rate than that of M. There as well, the environmental/structural change detected by the reporter group in position 35 appears to originate in M, but is associated with the M to N transition.

In summary, we have developed an experimental setup which allows the exploration of real-time dynamics and

environmental changes at the surface of membrane proteins. Especially the extension to time-resolved depolarization measurements enables the detection of single loop dynamics (20,21) during protein function. Applications to other light-activated proteins than bacteriorhodopsin (e.g. visual rhodopsin, proterhodopsin or sensory rhodopsin) and proteins with photo-inducible functions including protein-protein interactions are feasible and currently underway.

*Acknowledgements*—This work has been supported by grant Sfb 449 TP A5 of the Deutsche Forschungsgemeinschaft. We thank M. Möller for help by the photocycle measurements, I. Wallat for excellent technical assistance and M.P. Heyn for support and encouragement.

## REFERENCES

- Herbst, J., K. Heyne and R. Diller (2002) Femtosecond infrared spectroscopy of bacteriorhodopsin chromophore isomerization. *Science* **297**, 822–825.
- Bredenbeck, J., J. Helbing, A. Sieg, T. Schrader, W. Zinth, C. Renner, R. Behrendt, L. Moroder, J. Wachtveitl and P. Hamm (2003) Picosecond conformational transition and equilibration of a cyclic peptide. *Proc. Natl Acad. Sci. USA* **100**, 6452–6457.
- Bieri, O., J. Wirz, B. Hellrung, M. Schutkowski, M. Drewello and T. Kiefhaber (1999) The speed limit for protein folding measured by triplet-triplet energy transfer. *Proc. Natl Acad. Sci. USA* **96**, 9597–9601.
- Farrens, D. L., C. Altenbach, K. Yang, W. L. Hubbell and H. G. Khorana (1996) Requirement of rigid-body motion of transmembrane helices for light activation of rhodopsin. *Science* **274**, 768–770.
- Dunham, T. D. and D. L. Farrens (1999) Conformational changes in rhodopsin. Movement of helix F detected by site-specific chemical labeling and fluorescence spectroscopy. *J. Biol. Chem.* **274**, 1683–1690.
- Imamoto, Y., M. Kataoka, F. Tokunaga and K. Palczewski (2000) Light-induced conformational changes of rhodopsin probed by fluorescent alexa594 immobilized on the cytoplasmic surface. *Biochemistry* **39**, 15225–15233.
- Itoh, Y., K. Cai and H. G. Khorana (2001) Mapping of contact sites in complex formation between lightactivated rhodopsin and transducin by covalent crosslinking: Use of a chemically preactivated reagent. *Proc. Natl Acad. Sci. USA* **98**, 4883–4887.
- Cai, K., J. Klein-Seetharaman, J. Hwa, W. L. Hubbell and H. G. Khorana (1999) Structure and function in rhodopsin: Effects of disulfide cross-links in the cytoplasmic face of rhodopsin on transducin activation and phosphorylation by rhodopsin kinase. *Biochemistry* **38**, 12893–12898.
- Ernst, O. P., C. K. Meyer, E. P. Marin, P. Henklein, W. Y. Fu, T. P. Sakmar and K. P. Hofmann (2000) Mutation of the fourth cytoplasmic loop of rhodopsin affects binding of transducin and peptides derived from the carboxyl-terminal sequences of transducin alpha and gamma subunits. *J. Biol. Chem.* **275**, 1937–1943.
- Luecke, H., B. Schobert, H.-T. Richter, J.-P. Cartailler and J. K. Lanyi (1999) Structural changes in bacteriorhodopsin during ion transport at 2 Å resolution. *Science* **286**, 255–261.
- Sass, H. J., G. Bueldt, R. Gessenich, D. Hehn, D. Neff, R. Schlesinger, J. Berendzen and P. Ormos (2000) Structural alterations for proton translocation in the M state of wild-type bacteriorhodopsin. *Nature* **406**, 649–653.
- Subramaniam, S. and R. Henderson (2000) Molecular mechanism of vectorial proton translocation by bacteriorhodopsin. *Nature* **406**, 653–657.
- Vonck, J. (2000) Structure of the bacteriorhodopsin mutant F219L N intermediate revealed by electron crystallography. *EMBO J.* **19**, 2152–2160.
- Radzwill, N., K. Gerwert and H. J. Steinhoff (2001) Time-resolved detection of transient movement of helices F and G in doubly spin-labeled bacteriorhodopsin. *Biophys J.* **80**, 2856–2866.
- Oka, T., H. Kamikubo, F. Tokunaga, J. K. Lanyi, R. Needleman and M. Kataoka (1999) Conformational change of helix G in the bacteriorhodopsin photocycle: Investigation with heavy atom labeling and X-ray diffraction. *Biophys J.* **76**, 1018–1023.
- Brown, L. S., R. Needleman and J. K. Lanyi (2002) Conformational change of the E–F interhelical loop in the M photointermediate of bacteriorhodopsin. *J. Mol. Biol.* **317**, 471–478.
- Klein-Seetharaman, J., E. V. Getmanova, M. C. Loewen, P. J. Reeves and H. G. Khorana (1999) NMR spectroscopy in studies of light-induced structural changes in mammalian rhodopsin: Applicability of solution (19)F NMR. *Proc. Natl Acad. Sci. USA* **96**, 13744–13749.
- Crocker, E., M. Eilers, S. Ahuja, V. Hornak, A. Hirshfeld, M. Sheves and S. O. Smith (2006) Location of Trp265 in metarhodopsin II: Implications for the activation mechanism of the visual receptor rhodopsin. *J. Mol. Biol.* **357**, 163–172.
- Klare, J. P., E. Bordignon, M. Engelhard and H. J. Steinhoff (2004) Sensory rhodopsin II and bacteriorhodopsin: Light activated helix F movement. *Photochem. Photobiol. Sci.* **3**, 543–547.
- Alexiev, U., I. Rimke and T. Pöhlmann (2003) Elucidation of the nature of the conformational changes of the EF–interhelical loop in bacteriorhodopsin and of the helix VIII on the cytoplasmic surface of bovine rhodopsin: A time-resolved fluorescence depolarization study. *J. Mol. Biol.* **328**, 705–719.
- Schröder, G., U. Alexiev and H. Grubmüller (2005) Simulation of fluorescence anisotropy experiments: Probing protein dynamics. *Biophys. J.* **89**, 3757–3770.
- Yang, H., G. Luo, P. Karnachanaphaurach, T.-M. Louie, I. Rech, S. Cova, L. Xun and X. S. Xie (2003) Protein conformational dynamics probed by single-molecule electron transfer. *Science* **302**, 262–266.
- Mansoor, S., H. S. Mchaourab and D. L. Farrens (2002) Mapping proximity within proteins using fluorescence spectroscopy. A study of T4 lysozyme showing that tryptophan residues quench Bimane fluorescence. *Biochemistry* **41**, 2475–2484.
- Pöhlmann, T., R. A. Böckmann, H. Grubmüller, B. Uchanska-Ziegler, A. Ziegler and U. Alexiev (2004) Differential peptide dynamics is linked to major histocompatibility complex polymorphism. *J. Biol. Chem.* **279**, 28197–28201.
- Schmidt, M., R. Pahl, V. Srajer, S. Anderson, Z. Ren, H. Ihee, S. Rajagopal and K. Moffat (2004) Protein kinetics: Structures of intermediates and reaction mechanism from time-resolved x-ray data. *Proc. Natl Acad. Sci. USA* **101**, 4799–4804.
- Krebs, M. P., R. Mollaaghababa and H. G. Khorana (1993) Gene replacement in *Halobacterium halobium* and expression of bacteriorhodopsin mutants. *Proc. Natl Acad. Sci. USA* **90**, 1987–1991.
- Alexiev, U., R. Mollaaghababa, P. Scherrer, H. G. Khorana and M. P. Heyn (1995) Rapid long range proton diffusion along the surface of the purple membrane and delayed proton transfer into the bulk. *Proc. Natl Acad. Sci. USA* **92**, 372–376.
- Otto, H., T. Marti, M. Holz, T. Mogi, M. Lindau, H. G. Khorana and M. P. Heyn (1989) Aspartic acid-96 is the internal proton donor in the reprotonation of the Schiff base of bacteriorhodopsin. *Proc. Natl Acad. Sci. USA* **86**, 9228–9232.
- Scherrer, P. and W. Stoeckenius (1985) Effects of tyrosine-26 and tyrosine-64 nitration on the photoreactions of bacteriorhodopsin. *Biochemistry* **24**, 7733–7740.
- Mielke, T., U. Alexiev, M. Gläsel, H. Otto and M. P. Heyn (2002) Light-induced changes in the structure and accessibility of the cytoplasmic loops of rhodopsin in the activated MIII-state. *Biochemistry* **41**, 7875–7884.
- Lakowicz, J. R. (1999) *Principles of Fluorescence Spectroscopy*, 2nd ed., Plenum Press, New York.
- Becker, W. and A. Bergmann (2005) Multi-dimensional time-correlated single photon counting. In *Reviews in Fluorescence* (Edited by C. D. Geddes and J. R. Lakowicz), pp. 77–108. Springer Science and Business Media, New York.
- Becker, W., A. Bergmann, G. Biscotti and A. Rück (2004) Advanced time-correlated single photon counting technique for spectroscopy and imaging in biomedical systems. *Proc. SPIE* **5340**, 104–112.

34. Scherrer, P., U. Alexiev, T. Marti, H. G. Khorana and M. P. Heyn (1994) Covalently bound pH-indicator dyes at selected extracellular or cytoplasmic sites in bacteriorhodopsin. 1. Proton migration along the surface of bacteriorhodopsin micelles and its delayed transfer from surface to bulk. *Biochemistry* **33**, 13684–13692.
35. Mollaaghababa, R., H. J. Steinhoff, W. L. Hubbell and H. G. Khorana (2000) Time-resolved site-directed spin-labeling studies of bacteriorhodopsin: Loop-specific conformational changes in M. *Biochemistry* **39**, 1120–1127.